# Microscopic design of a synthetic spin-1 chain in an InAsP quantum dot array

Jacob Manalo<sup>®</sup>, \*Daniel Miravet<sup>®</sup>, and Pawel Hawrylak Department of Physics, University of Ottawa, Ottawa K1N 6N5, Canada

(Received 29 September 2022; revised 15 January 2024; accepted 19 January 2024; published 8 February 2024)

We present here the steps enabling the microscopic design of a synthetic spin-1 chain in an InAsP quantum dot (QD) array embedded in an InP nanowire. The chain is described by a two-leg multiorbital Hubbard Kanamori (HK) model with parameters obtained from the microscopic calculations of up to eight electrons in a single and double QD. In this HK model describing long arrays of QDs, using both exact diagonalization and matrix product state (MPS) tools, we demonstrate a fourfold quasidegenerate ground state separated from excited states by a finite energy gap similar to a Heisenberg spin-1 chain in the Haldane phase. We demonstrate characteristic behavior of spin- $\frac{1}{2}$  quasiparticles at the edges of the chain by observing the magnetic field dependence of the low-energy spectrum as a function of the applied magnetic field. The applied magnetic field isolates the singlet and  $S^z = 0$  triplet states from the other triplet components emulating a singlet-triplet qubit but with macroscopic quantum states. Most importantly, the regions in parameter space where the low-energy spectrum of the multiorbital Hubbard chain yields a Heisenberg spin-1 chain spectrum are mapped out.

## DOI: 10.1103/PhysRevB.109.085112

## I. INTRODUCTION

The development of solid-state quantum information processing devices and topological quantum matter is currently a research area of great interest [1-5]. At the moment, qubits developed for commercial use are superconducting [6-8], trapped ion [9,10], electron spin [11-14], and photonic qubits [15–17] due to their robustness and scalability [15,16,18-20]. Despite their merits, these qubits are not immune to the challenges of decoherence. Consequently, there is an ongoing quest to engineer topologically protected qubits that could potentially overcome these limitations [21-23]. There has also been recent interest in using spin chains as databuses [24-26] and spin clusters as coded qubits [27-29]. Spin-1 chains are prototypes of topological strongly correlated quantum matter hosting Haldane spin- $\frac{1}{2}$  quasiparticles [30–32] at its edges. Potential applications of spin- $\frac{1}{2}$  quasiparticles as qubits [21,33] have been suggested [33-35]. A synthetic spin-1 chain could be realized using gated triple quantum dots (QDs) [34], an array of semiconductor QDs in a nanowire [33,36], a chain of triangular graphene QDs [37-39], and in two-orbital Hubbard models [40]. Here, we discuss the atomistic design of a synthetic spin-1 chain hosting a macroscopic quantum state with Haldane quasiparticles using a semiconductor QD array in a nanowire filled with electrons.

Previous effective mass and Heisenberg-model-based spin calculations suggested that such a macroscopic quantum state can be realized using a chain of InAsP semiconductor QDs with four electrons each in a InP nanowire [21,33,36]. Furthermore, it has been shown through microscopic calculations that the ground state of a single InAsP QD in a nanowire is a spin

triplet and that the low-energy spectrum of an array of two InAsP QDs in an InP nanowire is similar to the spectrum of a Heisenberg chain of two spin-1 particles [36]. The parameters of this two-site Heisenberg Hamiltonian were used to extend the Heisenberg spin-1 chain.

Here, instead of an effective Heisenberg Hamiltonian, we derive and use an effective multiorbital Hubbard model with parameters obtained from microscopic atomistic calculations. We determine a set of microscopic parameters for which a long macroscopic QD chain with four electrons each has a fourfold quasidegenerate ground state separated from the quintuplet state by a finite energy gap, similar to a Heisenberg spin-1 chain. We also show that, at low energies, the electrons in a QD array behave the same way as two coupled spin- $\frac{1}{2}$  quasiparticles would in a magnetic field.

Furthermore, we show that the length of the array controls the singlet-triplet splitting, while the Zeeman splitting of the nonzero spin-triplet states allows us to isolate the quasidegenerate singlet and triplet states from the quintuplet allowing the two isolated states to emulate the two-electron singlet-triplet qubit [29,41]. We then demonstrate that the multiorbital Hubbard parameters which result in a Heisenberg spin-1 chain model form sizable regions in parameter space. Determining these parameters allows for the finetuning of the spectral gap. The parameters are tuned by controlling the size and As concentration of the InAsP QD as well as the interdot distance and material of the QD array enabling the construction of synthetic spin-1 chain.

The paper is organized as follows. First, we define the multiorbital Hubbard model in terms of individual QDs and the interaction between them. We then describe the methodology of the calculations which include exact diagonalization and density matrix renormalization group (DMRG) in the formalism of the matrix product state (MPS) [42–44] approach. Next, we analyze the low-energy spectrum as a function of

<sup>\*</sup>manalo@protonmail.com

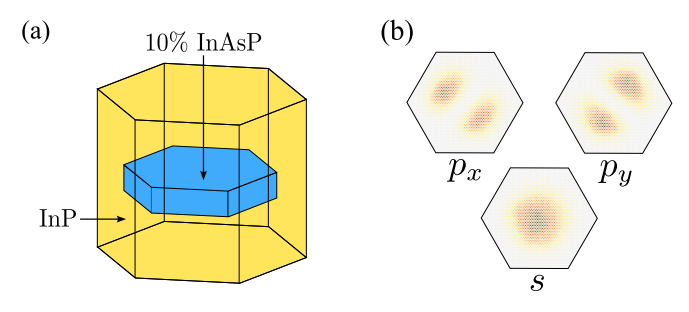


FIG. 1. (a) Hexagonal InAsP quantum dot (blue) in an InP nanowire (yellow). (b) Charge densities of single particle states.

array size and discuss the behavior of the chain in a magnetic field. Finally, we map out regions in parameter space where the multiorbital Hubbard model gives a low-energy spectrum that resembles that of the Heisenberg spin-1 chain.

## II. InAsP QD ARRAY IN AN InP NANOWIRE

We aim to realize a synthetic spin-1 chain with an array of InAsP QDs embedded in an InP nanowire. The QD array is constructed with a single InAsP QD shown in Fig. 1(a) as a building block. It has been shown that a synthetic spin-1 object is formed when four electrons are injected into the InAsP QD [36]. With each InAsP QD acting as a spin-1 object, we construct a synthetic spin-1 chain with an array of these InAsP QDs, as shown in Fig. 2.

The microscopic calculations for one and two InAsP QDs embedded in an InP nanowire serve as the foundation for the effective multiorbital Hubbard model that describes the InAsP QD array. Essentially, the microscopic calculations begin with *ab initio*-based tight-binding model [36,45–47] where the QD nanowire is created by first building an InP matrix and defining a hexagonal nanowire inside, as shown in Fig. 1(a), where random P atoms are replaced with As atoms at a concentration of, for example, 10%. Figure 1(b) shows the probability densities of the single-particle states obtained from the tight-binding model. Despite the random distribution of As atoms, the spectrum consists of a well-defined *s* shell followed by two states of a *p* shell.

Furthermore, it was shown that, when four electrons were inserted into the QD, two of the electrons filled the s shell, leaving the other two electrons to form a triplet state on the p shell. The many-body calculations of the N electron complex were done using the configuration interaction method for the

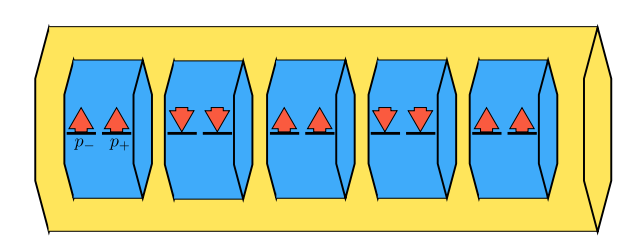


FIG. 2. A chain of InAsP quantum dots (blue) embedded in an InP nanowire (yellow). Red arrows indicate electrons with corresponding spin.

Hamiltonian given by

$$H_{MB} = \sum_{i} E_{i} c_{i}^{\dagger} c_{i} + \frac{1}{2} \sum_{ijkl} \langle ij|V|kl \rangle c_{i}^{\dagger} c_{j}^{\dagger} c_{k} c_{l}, \qquad (1)$$

where  $E_i$  is the energy of single particle state i,  $c_i^{\dagger}$  ( $c_i$ ) is the creation (annihilation) operator for an electron on state i, and  $\langle ij|V|kl\rangle$  is the Coulomb matrix element where two electrons, one in state i and another in state j, scatter to states k and l. Likewise, the many-body spectrum of two QDs, each with four electrons, resembled the spectrum of two coupled spin-1 particles. The limitation of these microscopic calculations extended to a long chain of QDs is that they are computationally expensive. Computing such arrays where each QD contains millions of atoms, with each atom containing 20 spin-up and spin-down orbitals, and four electrons per QD is presently not possible. Since the formation of Haldane quasiparticles requires a chain of many synthetic spin-1 quasiparticles, it is necessary to use a simplified model that still captures the physics of a spin-1 chain.

## III. THE MULTI-ORBITAL HUBBARD MODEL

We now turn to the effective multiorbital Hubbard model to describe the QD array shown in Fig. 2. In this model, each QD is described as a site with two p orbitals,  $p_-$  and  $p_+$ . Here, s-shell electrons are ignored because the probability of s electrons scattering to the p shell is negligible due to the large s-p splitting in the microscopic single-particle spectrum. Exchange interaction of additional two electrons half-filling the p shell can ferromagnetically couple their spins to form a synthetic spin-1 state, as shown schematically in Fig. 2.

To retain essential microscopic description of the QD, we reduce the microscopic Hamiltonian in Eq. (1) to the effective multiorbital Hubbard Hamiltonian for a single QD as given below:

$$H_0(i) = U_1 \sum_{\alpha} n_{i\alpha\uparrow} n_{i\alpha\downarrow} + \left( U_2 - \frac{J_{1/2}}{4} \right) n_{i-} n_{i+}$$
$$-J_{1/2} \mathbf{S}_{i-} \cdot \mathbf{S}_{i+} + \frac{\Delta}{2} \sum_{\alpha} \sum_{\alpha \neq \beta} c^{\dagger}_{i\alpha\sigma} c_{i\beta\sigma}, \qquad (2)$$

where  $\alpha, \beta \in \{-, +\}$  denote the orbital indices,  $\sigma \in \{\uparrow, \downarrow\}$  denotes spin, and  $n_{i\alpha} \equiv \sum_{\sigma} n_{i\alpha\sigma}$  is the number of electrons in orbital  $\alpha$  in QD i. This Hamiltonian, as well as the Hamiltonian for a chain of QDs, is derived from the microscopic Hamiltonian by employing certain approximations to the Coulomb matrix elements, as described in Ref. [36].

The first term is the Hubbard term, which describes the energy  $U_1$  required for spin-up and spin-down electrons to occupy a single orbital. The second term describes the coupling between electrons on the  $p_-$  and  $p_+$  shells with energy  $(U_2 - J_{1/2}/4)$ . Here,  $U_2$  is the direct Coulomb interaction between an electron on  $p_-$  and an electron on  $p_+$ , and  $J_{1/2}$  is the exchange between them. In general,  $U_1$  and  $U_2$  differ in value, but for the systems we are interested in,  $U_1 = U_2 \equiv U$ . The following  $J_{1/2}$  term describes the Heisenberg ferromagnetic coupling between  $p_-$  and  $p_+$  electrons, which is not to be confused with the effective Heisenberg spin-1 coupling between QDs, hence the subscript 1/2 in the coupling constant  $J_{1/2}$ .

This spin- $\frac{1}{2}$  coupling arises from the exchange interaction between electrons on different orbitals. Finally, the last term describes the p-shell splitting due to the broken lateral symmetry of the QD from the random distribution of As atoms, where the energy splitting  $\Delta$  is the splitting between the  $p_x$  and  $p_y$  orbitals which are both linear combinations of  $p_-$  and  $p_+$ .

To compute the spectrum of a chain of QDs, we must include the interaction between the QDs. The total multiorbital Hubbard Hamiltonian is now given by

$$H = \sum_{i} \left[ H_0(i) + t \sum_{\alpha\sigma} (c_{i\alpha\sigma}^{\dagger} c_{i+1\alpha\sigma} + \text{H.c.}) \right] + V \sum_{i} n_i n_{i+1},$$
(3)

which is the sum of all single-QD Hamiltonians in the array and the interactions between nearest-neighboring dots. The first term that describes the interdot interactions is the tunneling term  $tc^{\dagger}_{i\alpha\sigma}c_{i+1\alpha\sigma}$ , which describes the process of an electron hopping from QD i to the nearest-neighbor QD i+1 with a hopping energy t. The second term of the interdot interaction portion of the Hamiltonian describes the electrostatic interaction between electrons on neighboring QDs. Here,  $n_i \in [0,4]$  is the electron occupation of dot i, and V is the Coulomb matrix element, which is direct with respect to the dot index and is defined to be  $V \equiv \langle i\alpha, j\beta | V | j\beta, i\alpha \rangle$ , where  $\alpha, \beta \in \{p_+, p_-\}$ .

The two most important terms in determining the behavior of the system as a spin-1 chain are the intradot exchange term  $-J_{1/2}\sum_i \mathbf{S}_{i-} \cdot \mathbf{S}_{i+}$ , which describes the spin-spin coupling between a  $p_-$  electron and a  $p_+$  electron, and the tunneling term  $t\sum_i \sum_{\alpha\sigma} c^{\dagger}_{i\alpha\sigma} c_{i+1\alpha\sigma}$ . The intradot exchange term, which controls the electronic behavior of the QD as a spin-1 object is compromised by the tunneling term, which breaks the spin-1 apart. Without the interdot tunneling term, however, the singlet, triplet, and quintuplet states of the QD array will all be degenerate, which means that there is no finite gap in the spectrum.

The single dot parameters  $U_1$ ,  $U_2$ ,  $J_{1/2}$ , and  $\Delta$  and multidot parameters t and V were obtained by fitting the spectrum of Eq. (3) to the microscopic tight-binding spectrum of a two-dot array using a genetic algorithm. This effective multiorbital Hubbard model with parameters obtained from microscopic calculations allows us to simulate an array with many dots so that we can construct the synthetic spin-1 chain.

### IV. METHODOLOGY

In this paper, we compute the many-body spectrum of electrons in a large chain of QDs using the multiorbital Hubbard model and configuration interaction and DMRG tools to demonstrate the similarity to the spectrum of a spin-1 chain with two Haldane spin- $\frac{1}{2}$  quasiparticles. Next, we apply a magnetic field to the QD chain to determine the spin character of the Haldane spin- $\frac{1}{2}$  quasiparticles at the edges. Finally, regions in parameter space, i.e., the parameters in Eqs. (2) and (3), where the Hubbard chain produces a Heisenberg spin-1 chain spectrum, are mapped out.

All calculations of spectra of arrays with two QDs are done with exact diagonalization, while calculations

TABLE I. Multiorbital Hubbard parameters for the QD chain.

Parameter	Value (meV)
$\overline{U}$	15.971
$J_{1/2}$	5.000
$\Delta$	0.844
t	2.389
V	8.05

of spectra of larger arrays are done with the DMRG algorithm [42,43,44]. In this paper, we used iTensor and a tool that we developed called Python MPS (PyMPS) to perform the DMRG calculations [48,49].

Table I shows the multiorbital Hubbard model parameters that were obtained from microscopic calculations from our previous work of a double-QD array, where the dot diameter and height are 18.2 and 4.1 nm, respectively, and the interdot distance was taken to be 10 nm [36]. An important feature of the multiorbital Hubbard chain is the similarity of its low-energy spectrum and the spectrum of a spin-1 chain. However, the similarity to the spin-1 chain spectrum is dependent on the choice of multiorbital Hubbard parameters. This is evident with the example of a chain of two QDs. The spectrum of the two-QD array is shown in Fig. 3(a), where the parameters except for  $J_{1/2}$  and t are taken from Table I. While the Heisenberg spin-1 chain spectrum is reproduced with the parameters shown in Fig. 3(a), it is not reproduced when those parameters are changed, as shown in Fig. 3(b). The dependence of the spectrum on parameters allows us

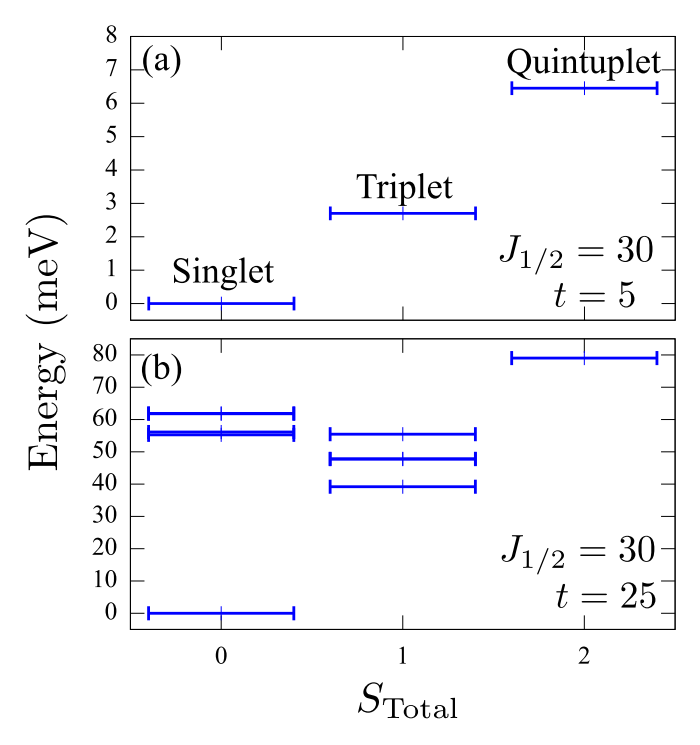


FIG. 3. Low-energy spectra of two quantum dots with two different sets of parameters. (a) The spectrum shows the spin-1 spectrum criterion satisfied, while (b) is an example where the criterion is not satisfied. All parameters are in meV.

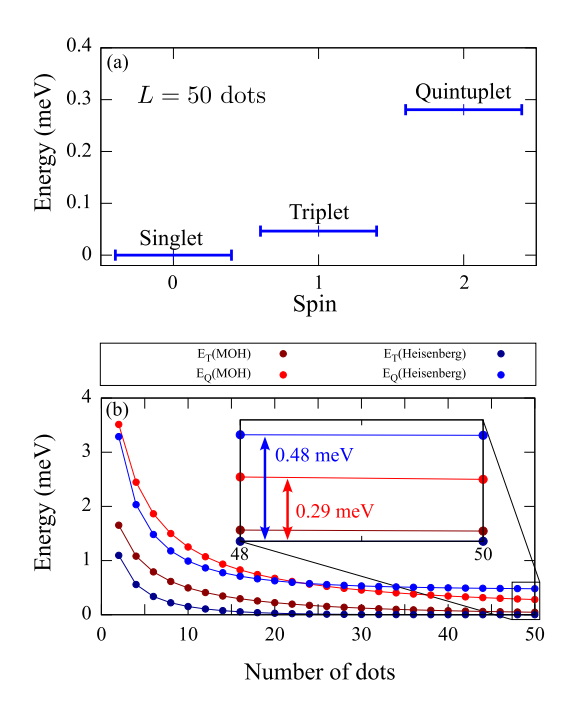


FIG. 4. Parameters used are in Table I. (a) Low-energy spectrum of a chain of 50 quantum dots (QDs) using the multiorbital Hubbard model (MOH). (b) Low-energy spectrum of a QD array as a function of array size using various models.  $E_T$  and  $E_Q$  denote triplet and quintuplet energies, respectively. All energies are shifted so that the singlet energy, which is not shown, is zero. The inset shows an enlarged section of the plot from L=48 to 50 dots.

to define a criterion for Heisenberg spin-1 chain behavior. The criterion is such that, when the multiorbital Hubbard spectrum replicates the spin-1 chain spectrum, as shown in Fig. 3(a), the criterion is satisfied; otherwise, as illustrated in Fig. 3(b), when the spectrum of the spin-1 chain is not replicated, the criterion is not satisfied. This principle applies to long arrays of QDs. For L = 50 QDs, the  $S^z = 0$  Hilbert space of the HK model at half-filling is  $\binom{100}{50}^2 \approx 10^{58}$ . For such a large Hilbert space, we apply MPS-DMRG tools to obtain the low-energy spectrum. Figure 4(a) shows an example where a chain of 50 QDs satisfies the spin-1 chain criterion. This criterion applies to any size of QD array and will be imperative to map out regions in parameter space where the system behaves as a chain of spin-1's.

The low-energy spectrum of the long chain shown in Fig. 4(a) illustrates the behavior of two uncoupled spin- $\frac{1}{2}$  quasiparticles. While Fig. 3(a) shows that the two-dot array resembles two spin-1's, Fig. 4(a) shows that the chain of many QDs resembles a chain of many spin-1 particles, which is understood in terms of two Haldane spin- $\frac{1}{2}$  quasiparticles at the edges. To illustrate the spectral gap, the spectrum of the multiorbital Hubbard Hamiltonian as a function of system size shown in Fig. 4(b) was computed and compared with that of the Heisenberg spin-1 chain.

The spectrum of the Heisenberg spin-1 chain was computed using the Heisenberg Hamiltonian given by

$$H = J_1 \sum_{i} \mathbf{S}_i \cdot \mathbf{S}_{i+1},\tag{4}$$

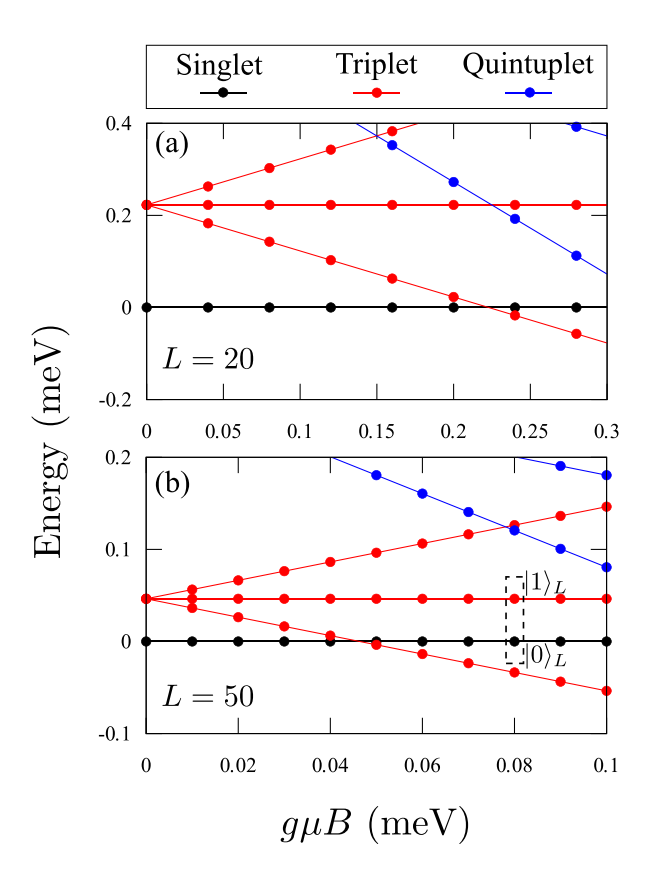


FIG. 5. Multiorbital Hubbard spectra as a function of magnetic field  $g\mu B$  for (a) L=20 and (b) L=50 quantum dot arrays. The  $S^z=0$  Haldane quasiparticle states are highlighted in the dashed square.

where  $J_1 = 2t^2/(U + \frac{J_{1/2}}{2} - V)$  is the effective Heisenberg spin-1 coupling, which is analytically obtained by treating the tunneling term in Eq. (3) as a perturbation [50].

We then added the term  $g\mu BS_{Total}^z$  to Eq. (3) to study the behavior of the QD array as a function of applied magnetic field. Using a chain of 20 and 50 QDs, we determined the array size required for the singlet-triplet splitting in Figs. 5(a) and 5(b) to be small enough to avoid unwanted level crossings.

Finally, to determine the set of multiorbital Hubbard parameters where the array gives a Heisenberg spin-1 chainlike spectrum, we set the following criterion: If the spectrum consists of a singlet ground state, followed by a triplet first excited state, then followed by a quintuplet second excited state with no other states in between, then the criterion is satisfied.

Figure 3 shows an example of a spectrum that satisfies the Heisenberg spin-1 criterion and another example that does not. In Fig. 3(a),  $t = \frac{1}{6}J_{1/2}$ , which is still in the perturbative regime, while in Fig. 3(b),  $t \sim J_{1/2}$ ; thus, the spin-1 description is no longer valid. Unlike the Heisenberg spin-1 chain spectrum, there are intermediate singlet and triplet states that appear below the quintuplet energy due to the coupling of the ground-state singlet and triplet to the higher-energy configurations that contain triple-electron occupation in a dot [36]. We then map out the regime in parameter space where this criterion is satisfied for a 16-QD system.

## V. RESULTS

One of the ways to determine the spin-1 chain characteristics of the QD array is to observe a quasidegenerate singlet-triplet ground state with a gap that separates the ground state from the quintuplet state in the low-energy spectrum. Like the multiorbital Hubbard spectrum for two QDs in Fig. 3(a), the spectrum of a chain of many dots in Fig. 4(a) also consists of a ground-state singlet followed by triplet and quintuplet states. The difference is that, unlike the spectrum of two QDs, the singlet and triplet states in the spectrum of the large chain are almost degenerate with a splitting of 0.05 meV and are separated by a spectral gap from the quintuplet state. The almost degenerate singlet-triplet states along with the spectral gap are indications of the existence of Haldane spin- $\frac{1}{2}$ quasiparticles at the edges. To demonstrate this point further, we show the energy of singlet and triplet states as a function of system size in Fig. 4(b). We see that the singlet and triplet become almost degenerate, while the singlet-quintuplet energy gap approaches a value of  $\sim 0.29$  meV.

The same behavior is observed in the spectrum of the Heisenberg spin-1 chain in Fig. 4(b), where the spectral gap is 0.45 meV. This spectral gap is known as the Haldane gap. Though the spectral gap for the multiorbital Hubbard model is only  $\sim$ 65% of the spectral gap in the Heisenberg spin-1 chain spectrum, this level of agreement is to be expected, considering the fact that the ground state of a two-dot multiorbital Hubbard model given these parameters is in  $\sim$ 70% agreement with the ground state of a two-site Heisenberg spin-1 chain, as seen in the overlap integral which was calculated in Ref. [36]. Next, we apply a magnetic field by adding Zeeman energy to demonstrate that the QD array behaves the same way as two spin- $\frac{1}{2}$  particles would in a magnetic field and to show that the  $S^z = 0$  triplet and singlet can be isolated in analogy with two electron singlet-triplet qubit basis. The spectra for 20 and 50 QD arrays as a function of an applied magnetic field are shown in Fig. 5. In both the L = 20 and 50 cases, the Zeeman splitting between the triplet components increases as a function of magnetic field, while the singlet remains unaffected, which is also the case for two coupled spin- $\frac{1}{2}$  particles. With the inclusion of the Zeeman splitting of the quintuplet components, this system behaves as a Heisenberg spin-1 chain would under a magnetic field.

For the low-energy spectrum made of Haldane quasiparticles, we expect the  $S^z = \pm 1$  triplet components to split away and isolate the  $S^z = 0$  triplet and singlet in a magnetic field. At higher energy, we expect quintuplet states outside the Haldane quasiparticle manifold. The  $S^z = -2$  quintuplet made of spin-1 states crosses the  $S^z = 0$  triplet made of Haldane quasiparticles. This does not happen with the L=20 chain, as seen in Fig. 5(a), where at about  $g\mu B = 0.24$  meV, the  $S^z = -1$  triplet begins to cross below the singlet, but by then, the lowest-energy quintuplet already crossed below the  $S^z = 0$ triplet. For the L = 50 chain, the singlet-triplet splitting at zero fields is small enough such that isolation of the zero singlet and triplet occurs before any quintuplet crossing occurs. At about  $g\mu B = 0.07$  meV, as seen in Fig. 5(b), the nonzero triplets isolate the  $S^z = 0$  states before the lowest-energy quintuplet crosses even the  $S^z = +1$  triplet.

Spin-1 chain regime diagrams for 2 dots

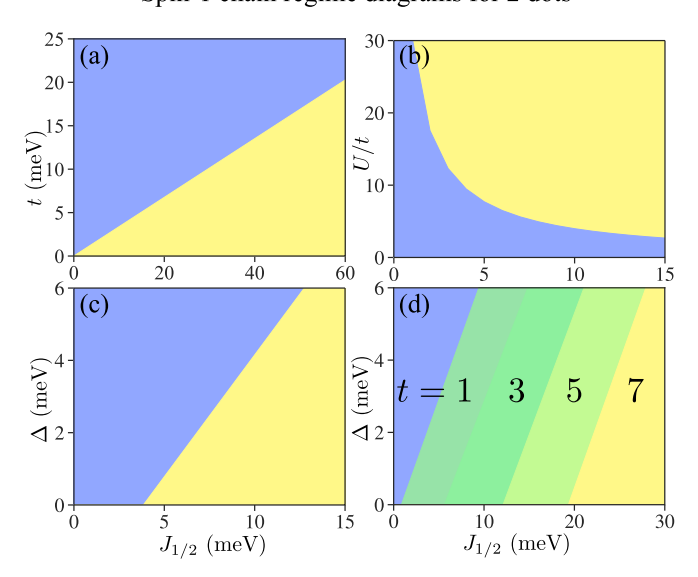


FIG. 6. Spin-1 chain spectrum criterion as a function of various multiorbital Hubbard parameters for an array of two quantum dots. Yellow (or green) region is where the criterion is satisfied, and blue is otherwise. (a) Diagram of t and  $J_{1/2}$ , (b) diagram of U/t and  $J_{1/2}$ , (c)  $\Delta$  vs  $J_{1/2}$  and (d)  $\Delta$  vs  $J_{1/2}$  at different values of t, where all the values of t are in units of meV.

It is also useful to construct a synthetic spin-1 chain with other parameters. These multiorbital Hubbard parameters depend on the material, QD As concentration, interdot distance, and QD size. Varying these parameters would vary the spectral gap since  $J_1 \propto \frac{t^2}{U + \frac{J_{1/2}}{2} - V}$  [50]; hence, it is important to find which parameters would yield a synthetic spin-1 chain.

We map out regions in parameter space for 2- and 16-dot arrays, where the Hamiltonian in Eq. (3) produces a spin-1 chain spectrum, that is, regions where the spectrum consists of a singlet ground state, a triplet first excited state, and a quintuplet second excited state. In both Figs. 6 and 7, there are clear regions in parameter space where a spin-1 spectrum is produced as opposed to random points sporadically dispersed. We decided to omit the parameter *V* from the diagrams because the term containing this factor only contributes a constant shift to the low-energy spectrum due to all of the orbitals in these states having single occupation.

In Fig. 6(a), we see a tunneling matrix element t varying linearly with  $J_{1/2}$  at the boundary. Moreover, Fig. 6(b) shows a  $\frac{1}{J_{1/2}}$  dependence of U at the boundary, which is expected because of the linear dependence of t on  $J_{1/2}$  at the boundary in Fig. 6(a). In Fig. 6(c), we see a linear dependence between  $\Delta$  and J at the boundary. Furthermore, varying t at different cross-sections of the  $\Delta$ - $J_{1/2}$  plane, as shown in Fig. 6(d), does not vary the slope of the boundary. However, the  $J_{1/2}$  intercept increases with t.

Since the appearance of Haldane quasiparticles requires long chains, we also map out regions in parameter space where a spin-1 chain spectrum is produced for a 16 dot system in Fig. 7. Similar trends to the 2-dot diagrams are seen in the 16-dot diagrams. For instance, linear dependence of t on  $J_{1/2}$ 

# Spin-1 chain regime diagrams for 16 dots

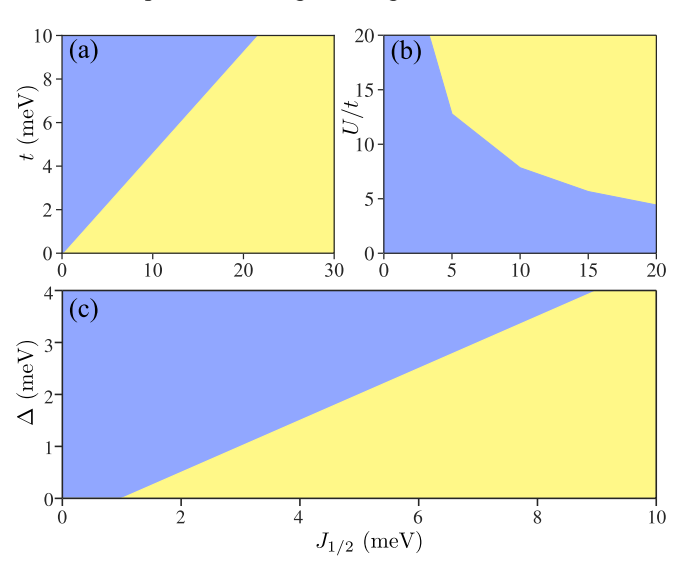


FIG. 7. Spin-1 spectrum criterion as a function of various multiorbital Hubbard parameters for an array of 16 quantum dots. Yellow region is where the criterion is satisfied, and blue is otherwise. All parameters are the same as the ones used in Figs. 4 and 5 except for those that are varied.

at the boundary where the spin-1 chain criterion is satisfied is shown in Fig. 7(a). The  $\frac{1}{J_{1/2}}$  dependence in Fig. 7(b) is also seen as well as the linear dependence of  $\Delta$  on  $J_{1/2}$  in Fig. 7(c).

The two lowest-energy eigenstates for a single QD with two electrons in the p shell are a triplet ground state and a singlet first excited state separated by an energy  $E_{s1} = \frac{3J_{1/2} - \sqrt{J_{1/2}^2 + (4\Delta)^2}}{4}$  [36]. If another QD is placed beside the first one, the orbitals in different dots are coupled by the hopping term  $tc_{i\alpha}^{\dagger}c_{i+1\alpha}$ . We see the effect of hopping in the spectrum of four electrons on two QDs in the splitting of the singlet and triplet double QD states, where in this case, the singlet is the ground state and the first excited state is a triplet. In the regime where the hopping term in Eq. (3) is weak, the singlet-triplet splitting is proportional to the effective Heisenberg spin-1 coupling  $J_1 = 2t^2/(U + J_{1/2}/2 - V)$ . This introduces the condition  $J_1 < E_{s1}$ , which can be interpreted as the values of t which conserve the spin-1 character of each QD in the array. This condition can shed light on Figs. 6 and 7.

Increasing  $J_{1/2}$  increases the singlet-triplet splitting for a single QD, protecting the spin-1 character of each dot against perturbations according to the analytic expression of  $E_{s1}$ . This behavior is observed in Figs. 6 and 7, where the Haldane phase is favored whenever  $J_{1/2}$  is increased. On the other hand, an increase in the hopping energy t mixes the single QD ground and excited states, destabilizing the Haldane phase, which is also observed in Figs. 6(a) and 7(a). Similarly, increasing the p-shell splitting  $\Delta$  decreases the singlet-triplet gap in a single QD, eventually producing a ground state that is a singlet instead of a triplet in the case when  $E_{s1} < 0$ , losing the spin-1 behavior of each QD.

In Figs. 6(c) and 7(d), the competition between  $J_{1/2}$  and  $\Delta$  terms can be seen directly. Particularly, in Fig. 6(d), the

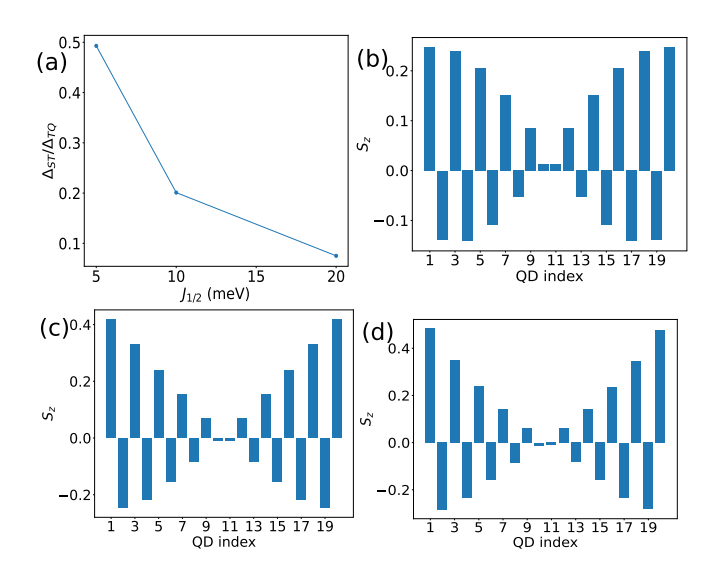


FIG. 8. (a) Ratio between the singlet-triplet and triplet-quintuplet gaps  $\Delta_{ST}/\Delta_{TQ}$  for a chain with a length of L=20 as a function of  $J_{1/2}$ . Expectation value of magnetization per quantum dot (QD) in the state  $|S,S_z\rangle=|1,1\rangle$ , for (b)  $J_{1/2}=5$  meV, (c)  $J_{1/2}=10$  meV, (d)  $J_{1/2}=20$  meV, edge states with  $s_z\sim\frac{1}{2}$  are present at the ends of the chain.

combined effect of varying  $\Delta$  with the hopping term t and  $J_{1/2}$  is shown. When the hopping energy t is increased,  $J_{1/2}$  must also increase even for negligible  $\Delta$  to stabilize the Haldane phase. This is the reason behind the increasing of the  $J_{1/2}$  intercept as t increases.

In Fig. 8(a), we present the ratio between the singlet-triplet gap  $\Delta_{ST}$  and triplet-quintuplet gap  $\Delta_{TQ}$  as a function of  $J_{1/2}$ for a chain with a length of L = 20. As  $J_{1/2}$  increases, the ratio decreases. This observation aligns with the concept we previously discussed regarding the influence of  $J_{1/2}$  on isolating the spin-1 character of the QD. Furthermore, Figs. 8(b)-8(d) show the expectation value of magnetization per QD in the state  $|S, S_z\rangle = |1, 1\rangle$ , revealing a clearer spin- $\frac{1}{2}$  edge fractionalization for the larger value of  $J_{1/2}$ , which is characteristic of a Haldane chain [51]. Remarkably, while individual spins are limited to magnetization values of  $0, \pm 1$ , this result shows the emergence of spin- $\frac{1}{2}$  quasiparticles localized at the edges of the chain. As the chain length increases, the coupling between these  $\frac{1}{2}$  quasiparticles decreases, elucidating the degeneracy observed between triplet and singlet states in macroscopic chains.

#### VI. CONCLUSIONS

We presented here the steps enabling the microscopic design of a synthetic spin-1 chain in an InAsP QD array. The multiorbital Hubbard model derived from a microscopic atomistic Hamiltonian is used to describe the electronic spectrum. A degenerate singlet-triplet ground state followed by a spectral gap separating the ground state from the quintuplet state is observed in the low-energy spectrum of the multiorbital Hubbard chain. This behavior is also observed in the spectrum of a Heisenberg spin-1 chain, indicating the existence of spin- $\frac{1}{2}$  Haldane quasiparticles at the edges of the chain. Further indication of the existence of spin- $\frac{1}{2}$ 

quasiparticles is the behavior of the low-energy spectrum as a function of applied magnetic field. Despite the system being a chain of synthetic spin-1's constructed using an InAsP QD array with exponentially growing Hilbert space, the magnetic field dependence of the spectrum is the same as that of two spin- $\frac{1}{2}$  quasiparticles. The external magnetic field also allows the  $S^{z}=0$  triplet and singlet quasiparticle states to be isolated, emulating states of an electronic singlet-triplet qubit. For the design of Haldane quasiparticles, the regions in parameter space where the low-energy spectrum of the Heisenberg spin-1 chain is reproduced with the multiorbital Hubbard model are mapped out.

## ACKNOWLEDGMENTS

The authors thank Y. Núñez-Fernández and Hassan Allami for useful discussions. This paper was supported by Natural Sciences and Engineering Research Council of Canada (NSERC) QC2DM Strategic Grant No. STPG-521420, NSERC Discovery Grant No. RGPIN-2019-05714, National Research Council Canada Applied Quantum Computing AQC 004 Challenge Program, and University of Ottawa Research Chair in Quantum Theory of Materials, Nanostructures, and Devices. This paper was enabled in part by support provided by the Digital Research Alliance of Canada [52].

- [1] M. Korkusinski and P. Hawrylak, Coded qubits based on electron spin, in *Semiconductor Quantum Bits* (Pan Stanford Publishing, Boca Raton, 2008), Chap. 1, pp. 3–32.
- [2] A. Alfieri, S. B. Anantharaman, H. Zhang, and D. Jariwala, Adv. Mater. 35, 2109621 (2022).
- [3] C. Kloeffel and D. Loss, Annu. Rev. Condens. Matter Phys. 4, 51 (2013).
- [4] T. E. Northup and R. Blatt, Nat. Photon. 8, 356 (2014).
- [5] P. Laferrière, E. Yeung, M. Korkusinski, P. J. Poole, R. L. Williams, D. Dalacu, J. Manalo, M. Cygorek, A. Altintas, and P. Hawrylak, Appl. Phys. Lett. 118, 161107 (2021).
- [6] M. W. Johnson, M. H. S. Amin, S. Gildert, T. Lanting, F. Hamze, N. Dickson, R. Harris, A. J. Berkley, J. Johansson, P. Bunyk *et al.*, Nature (London) 473, 194 (2011).
- [7] J. M. Gambetta, J. M. Chow, and M. Steffen, npj Quantum Inf. 3, 2 (2017).
- [8] F. Arute, K. Arya, R. Babbush, D. Bacon, J. C. Bardin, R. Barends, R. Biswas, S. Boixo, F. G. S. L. Brandao, D. A. Buell *et al.*, Nature (London) **574**, 505 (2019).
- [9] K. Wright, K. M. Beck, S. Debnath, J. M. Amini, Y. Nam, N. Grzesiak, J.-S. Chen, N. C. Pisenti, M. Chmielewski, C. Collins *et al.*, Nat. Commun. 10, 5464 (2019).
- [10] I. Pogorelov, T. Feldker, C. D. Marciniak, L. Postler, G. Jacob, O. Krieglsteiner, V. Podlesnic, M. Meth, V. Negnevitsky, M. Stadler *et al.*, PRX Quantum 2, 020343 (2021).
- [11] J. A. Brum and P. Hawrylak, Superlattices Microstruct. 22, 431 (1997).
- [12] D. Loss and D. P. DiVincenzo, Phys. Rev. A 57, 120 (1998).
- [13] T. Kobayashi, J. Salfi, C. Chua, J. van der Heijden, M. G. House, D. Culcer, W. D. Hutchison, B. C. Johnson, J. C. McCallum, H. Riemann *et al.*, Nat. Mater. 20, 38 (2021).
- [14] F. H. L. Koppens, C. Buizert, K. J. Tielrooij, I. T. Vink, K. C. Nowack, T. Meunier, L. P. Kouwenhoven, and L. M. K. Vandersypen, Nature (London) 442, 766 (2006).
- [15] E. Knill, R. Laflamme, and G. J. Milburn, Nature (London) **409**, 46 (2001).
- [16] L. S. Madsen, F. Laudenbach, M. F. Askarani, F. Rortais, T. Vincent, J. F. F. Bulmer, F. M. Miatto, L. Neuhaus, L. G. Helt, M. J. Collins *et al.*, Nature (London) **606**, 75 (2022).
- [17] P. Kok, W. J. Munro, K. Nemoto, T. C. Ralph, J. P. Dowling, and G. J. Milburn, Rev. Mod. Phys. 79, 135 (2007).
- [18] A. H. Myerson, D. J. Szwer, S. C. Webster, D. T. C. Allcock, M. J. Curtis, G. Imreh, J. A. Sherman, D. N. Stacey, A. M. Steane, and D. M. Lucas, Phys. Rev. Lett. 100, 200502 (2008).

- [19] F. Hassler, A. R. Akhmerov, and C. W. J. Beenakker, New J. Phys. 13, 095004 (2011).
- [20] A. Martin, B. Candelas, A. Rodríguez-Rozas, J. D. Martín-Guerrero, X. Chen, L. Lamata, R. Orús, E. Solano, and M. Sanz, Phys. Rev. Res. 3, 013167 (2021).
- [21] B. Jaworowski and P. Hawrylak, Appl. Sci. 9, 474 (2019).
- [22] J. D. Sau and S. D. Sarma, Nat. Commun. 3, 964 (2012).
- [23] R. M. Lutchyn, E. P. A. M. Bakkers, L. P. Kouwenhoven, P. Krogstrup, C. M. Marcus, and Y. Oreg, Nat. Rev. Mater. 3, 52 (2018).
- [24] M. Friesen, A. Biswas, X. Hu, and D. Lidar, Phys. Rev. Lett. **98**, 230503 (2007).
- [25] S. Oh, Y.-P. Shim, J. Fei, M. Friesen, and X. Hu, Phys. Rev. B 85, 224418 (2012).
- [26] N. Chancellor and S. Haas, New J. Phys. 14, 095025 (2012).
- [27] F. Meier, J. Levy, and D. Loss, Phys. Rev. B 68, 134417 (2003).
- [28] X. Wu, D. R. Ward, J. R. Prance, D. Kim, J. K. Gamble, R. T. Mohr, Z. Shi, D. E. Savage, M. G. Lagally, M. Friesen *et al.*, Proc. Natl. Acad. Sci. USA 111, 11938 (2014).
- [29] J. Levy, Phys. Rev. Lett. 89, 147902 (2002).
- [30] F. D. M. Haldane, Phys. Lett. A 93, 464 (1983).
- [31] F. D. M. Haldane, Rev. Mod. Phys. 89, 040502 (2017).
- [32] I. Affleck, T. Kennedy, E. H. Lieb, and H. Tasaki, Phys. Rev. Lett. **59**, 799 (1987).
- [33] B. Jaworowski, N. Rogers, M. Grabowski, and P. Hawrylak, Sci. Rep. 7, 5529 (2017).
- [34] Y.-P. Shim, A. Sharma, C.-Y. Hsieh, and P. Hawrylak, Solid State Commun. 150, 2065 (2010).
- [35] C.-Y. Hsieh, Y.-P. Shim, M. Korkusinski, and P. Hawrylak, Rep. Prog. Phys. 75, 114501 (2012).
- [36] J. Manalo, M. Cygorek, A. Altintas, and P. Hawrylak, Phys. Rev. B 104, 125402 (2021).
- [37] A. D. Guclu, P. Potasz, M. Korkusinski, and P. Hawrylak, *Graphene Quantum Dots* (Springer, Berlin, 2014).
- [38] S. Mishra, G. Catarina, F. Wu, R. Ortiz, D. Jacob, K. Eimre, J. Ma, C. A. Pignedoli, X. Feng, P. Ruffieux *et al.*, Nature (London) 598, 287 (2021).
- [39] G. Catarina and J. Fernández-Rossier, Phys. Rev. B 105, L081116 (2022).
- [40] A. Jażdżewska, M. Mierzejewski, M. Środa, A. Nocera, G. Alvarez, E. Dagotto, and J. Herbrych, Nat. Commun. 14, 8524 (2023).
- [41] C. Barthel, D. J. Reilly, C. M. Marcus, M. P. Hanson, and A. C. Gossard, Phys. Rev. Lett. 103, 160503 (2009).

- [42] S. R. White, Phys. Rev. Lett. 69, 2863 (1992).
- [43] U. Schollwöck, Rev. Mod. Phys. 77, 259 (2005).
- [44] F. Verstraete, D. Porras, and J. I. Cirac, Phys. Rev. Lett. 93, 227205 (2004).
- [45] M. Zieliński, M. Korkusiński, and P. Hawrylak, Phys. Rev. B 81, 085301 (2010).
- [46] W. Sheng and P. Hawrylak, Phys. Rev. B 72, 035326 (2005).
- [47] M. Cygorek, M. Korkusinski, and P. Hawrylak, Phys. Rev. B **101**, 075307 (2020).
- [48] M. Fishman, S. R. White, and E. M. Stoudenmire, SciPost Phys. Codebases 4 (2022).
- [49] J. Manalo and D. Miravet, Python matrix product states DMRG tool (2021), available at https://github.com/jacobmanalo/dmrg\_ tool/
- [50] B. Jaworowski, Electron Correlations in Topological Flat Bands, Ph.D. thesis, Wroclaw University of Science and Technology 2018.
- [51] S. R. White, Phys. Rev. B 48, 10345 (1993).
- [52] alliancecan.ca.